Proceedings of International Conference on Heat Exchanger Fouling and Cleaning - 2013 (Peer-reviewed)
June 09 - 14, 2013, Budapest, Hungary
Editors: M.R. Malayeri, H. Müller-Steinhagen and A.P. Watkinson
Published online
www.heatexchanger-fouling.com

FOULING OF A HEATED ROD IN A STIRRED TANK SYSTEM

B. Petkovic and A.P. Watkinson[1]
Department of Chemical and Biological Engineering, The University of British Columbia
Vancouver, BC Canada V6T 1Z3.

[1]apw@chbe.ubc.ca

ABSTRACT

A batch stirred tank device has been developed for measuring fouling. The unit consists of a baffled tank equipped with a centrally-mounted long blade stirrer, and an electrically heated rod located at 40% of the radius of the tank. Heat transfer from the rod was first characterized. The velocity field was measured, which allowed the wall shear on the heating probe to be calculated. Micron sized iron oxide particles were added to a heavy oil fraction, and fouling was studied with bulk oil temperatures typically at 320°C, initial probe surface temperatures to 536°C, and stirrer speeds of 100─900 rpm. Deposition rates were measured thermally from the change in heat transfer coefficient when fouling was relatively heavy, and by thickness and mass accumulation when fouling was light. Effects of process variables on deposition rate and deposit composition are presented. Mass deposition rate increases with film temperature yielded a fouling activation energy of 53 kJ/mol. Rates declined with increasing rotational speed above 200 rpm, or wall shear stresses above a few Pascals.

INTRODUCTION

No single device has been universally accepted to measure fouling rates in a laboratory setting, as most test methods have disadvantages as well as advantages. For industrial fluids such as petroleum oils, desirable features of a fouling test apparatus include: apparatus should be operable at relatively high temperatures and pressures, and able to detect small extents of fouling; required fluid sample volume should be small; deposits should be accessible for examination of structure; and heating surface material should be readily changeable. In addition, the flow field within the test unit should be known such that Reynolds number or wall shear stress can be determined, and preferably be in a range that can be applicable to industrial heat exchangers or fired furnaces.

Although the compact Alcor HLPS system meets many of the above desirable features (Fan et al., 2010), turbulent flow conditions are not attained in the test section. For tubular or annular flow sections with external feed tanks and pumps, turbulent flows usually require substantially larger equipment and liquid samples (Srinivasan and Watkinson, 2005; Bennett et al., 2009). Rotary systems are prominent among recent developments, such as the stationary heated probe with rotating shell developed by Young et al. (2009), the isothermal rotating cylinder mass deposition unit of Akbarzadeh et al. (2012), and the rotary mixed heated-wire apparatus of Stephenson et al. (2011).

An alternative to these methods, based on a stirred tank and commonly available heating probes was developed in this work. Here the focus was on small liquid sample size, simplicity of stirrer system, inexpensive and replaceable heating probes, and an ability to operate over temperatures into the coking range for heavy oils. The method is not without its drawbacks. The major ones are the complexity of flow around the vertical cylinder, and the necessity to link the flow field from the central mixer to the adjacent heating probe, such that the Reynolds number over the heated rod and the surface shear stress could be determined.

APPARATUS AND PROCEDURES

Stirred Tank Fouling Unit The heart of the system (Figure 1) is the stirred tank (ID = 13 cm, depth 11 cm, Volume 1.5L) with two immersed 11.4 cm long cylindrical cartridge heater rods (probes). Some early work (e.g. in Fig. 3) used a tank depth of 18 cm and longer probes. Four baffles of 10 mm width, and a cooling coil were placed in the tank. One probe, with a thermocouple in its core, is heated and behaves as a fouling sensing element. An unheated "dummy" probe is positioned opposite to the heated rod to create a symmetrical flow field. Probes were placed tangentially midway between the baffles. A flat-bladed impeller (dia. 45 mm), with four blades of 90 mm length, and stirred using a Caframo mixer drive, was designed to create a uniform flow over the probe length (heated length of 94 mm), with minimal axial mixing. Visualization tests with a non-heated Lucite system showed that flow occurs in radial concentric circles, with velocity decreasing from the mixer tip toward the tank wall.

Various commercial heating rods were tested in this work. Desired features (Fig. 2) included: Rating 1000 W at 120 V, 316 SS or Incoloy 800 sheath material, 9.5 mm dia. with 114 mm (4.5") insert length, and a 20 mm long unheated section to pass through the tank lid, a uniformly distributed wattage with no cold sections, and a type K thermocouple, located in the radial and axial centre of the cartridge. Type 1 probes lacked the 20 mm unheated top section, and resulted in bulky deposits where the probe passed through the tank lid. Type 2 Incoloy 800 probes, which met all the above desired features were supplied by Gordo Sales, Utah, USA. The casing of the probe (outer diameter 9.5 mm, inner diameter 7.7 mm) contains the heating coil (wire diameter 0.3 mm, coil outside diameter

5.7mm) and is packed with magnesium oxide. Probe Reynolds numbers (based on approach velocity and film temperature) were in the turbulent regime (2,200<Re<20,800), as rotation speeds ranged from 100 to 900 revolutions/minute.

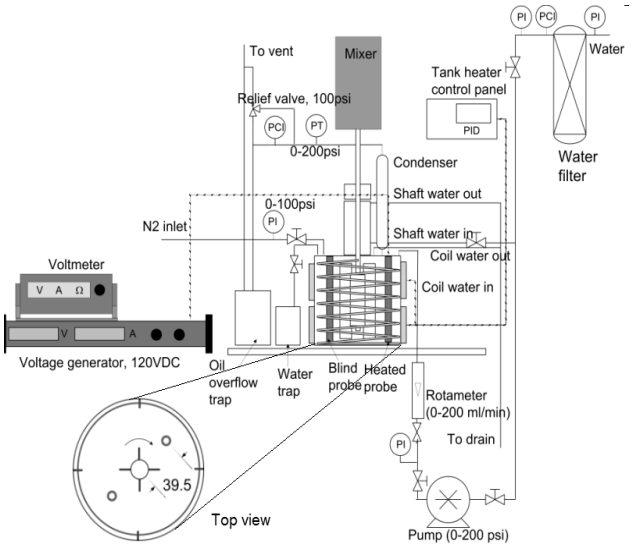

Fig. 1 Schematic diagram of stirred tank fouling unit

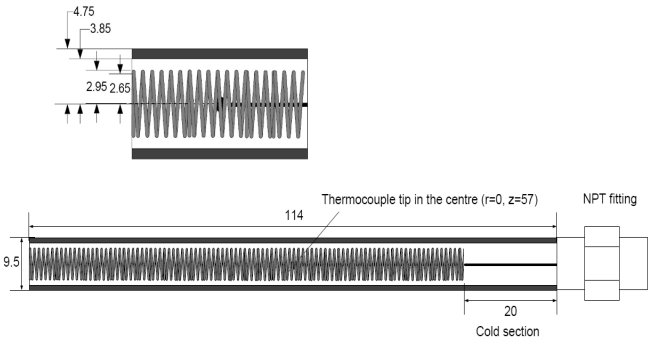

Fig. 2 Fouling probe schematic (units in mm.)

The overall heat transfer coefficient is based on the temperatures in the core of the heater, and the bulk fluid, $U=q/(T_{core}-T_b)$; surface temperatures are calculated from a conduction model, or via a Wilson-plot method (Fernández-Seara et al., 2007). Heated probe temperature rise indicates the extent of fouling, since formation of deposits on the probe surface, at constant heat flux and heat transfer coefficient, leads to an increase in the measured temperature. A DC power supply, maintained the current constant at ±0.1% of the nominal value. Voltage from the generator was measured and logged using a multi-meter. All temperatures on the unit were measured using K-type thermocouples, and logged on a computer.

Procedures, Materials and Calculations Two atmospheric tower bottoms (ATB) oil samples were used (Table 1). The tank was filled to the top with oil (allowing for expansion). Heating and maintaining a desired oil bulk temperature was achieved through control of upper and lower external tank heaters. Cooling water at a regulated pressure was used to balance the probe heat duty. To prevent auto-oxidation the heavy oil was purged with nitrogen before each experiment; to prevent sub-cooled boiling during the experiment, the tank was kept pressurized with nitrogen at 377 kPa (40 psig). During the experiment, hydrocarbon vapors develop due to evaporation of lighter components present in oil (maximum T_b= 360°C), or due to thermal cracking at the probe surface (maximum $T_{s,0}$= 536°C). Condensable vapor components were returned to the vessel, while the remaining vapors were sent to the backpressure regulator (set at 411 kPa), and exhausted through an oil overflow trap. Mechanical shaft design of the current unit limited proper sealing to 445 kPa.

Iron oxide particles (Fe_2O_3) of nominal size <5 microns from SigmaAldrich were used in the majority of experiments. A second sample of nominal size <1 micron was also obtained. Optical microscopy of a thin film of ATB with particles added showed that the volumetric mean diameter of particles was 2.0 and 1.6 microns, respectively for the two iron oxide samples. For fouling experiments, particles were dispersed in the oil by low-speed blending with a propeller mixer, followed by ten minutes of high-shear mixing at 6000 rpm.

The rate of deposit accumulation on the probe can be expressed as:

$$\frac{dR_f}{dt} = \frac{d\left(\frac{1}{U}\right)}{dt} = \frac{\frac{dx}{dt}}{\lambda_d} = \frac{\frac{dm}{dt}}{\rho_d \lambda_d} \qquad (1)$$

Table 1 Properties and Comparative Fouling Rates for Two Oils

Oil Designation	ATB1	ATB2
° API	14.3	24.1
Pentane Insolubles (wt.%)	5.8	1.4
Toluene Insolubles (wt.%)	0.2	0.3
Sulphur (wt.%)	3.5	0.6
Conradson Carbon (wt.%)	8.7	3.4
Suspended solids (ppm by D4807)	280	355
Density at 40°C and 80°C (kg/m3)	960, 936	894, 869
Viscosity at 40°C and 80°C (mPa.s)	460, 50	280, 39
Fixed carbon by TGA (wt.%)	5.3	0.2
Depos'n rate (mg/day) at $T_{s,o}$= 454°C at $T_{s,o}$= 505°C	42 135	16.5 23

After a run, the system was cooled to 50°C, the probe was washed with varsol solvent to remove oil, dried at 110°C for 30 minutes to remove the solvent, and the probe photographed, weighed, its diameter measured with a mechanical micrometer to obtain local axial and azimuthal variation in deposit thickness from which an average value of d*x*/d*t* was determined over 24 hours. Samples of the deposit were removed mechanically for analysis. For many conditions, thermal deposition rates were very low, and roughness effects were present, which obviated simple interpretation of surface temperature data. Hence, deposition rates are expressed by mass accumulation rate. Similar trends were found of dx/dt and dm/dt with process variables.

The surface temperature was calculated from the core temperature via a one-dimensional radial conduction equation, which accounted for the location of the coil, the MgO packing, and the metal wall of the probe. This method was checked by a Wilson-plot method (Fernández-Seara et al., 2007), in which 1/U is plotted versus $(1/V_p)^b$ to determine the combined thermal resistance of the probe insulation plus metal sheath, referred to as the wall resistance. With b= 0.62, a wall thermal resistance 35% above that of the model was found; at b=0.55, the model value was matched. Given some uncertainties in the Wilson-plot method, the thermal conduction model value of R_w/A_o = 0.045 (K/W) was adopted to calculate surface temperatures from measured core temperatures.

FLUID FLOW AND HEAT TRANSFER

Measurements of the radial velocity profile in the tank The velocity in the tank will decrease with distance in the radial direction from the impeller tip, and the approach velocity profile to the probe will not be uniform over its perimeter. Since the probe diameter is not too large compared to the tank radius (9.5 mm vs. 64.5 mm), the uneven approach velocity profile can be approximated as a flat profile, having the same velocity as would exist at the center of the probe. Although this results in a symmetrical profile of the shear stress, it was considered to be a satisfactory approximation for the average shear stress calculation.

Pitot tubes (Tropea et al., 2007) were used to measure local fluid velocity. Point velocities were determined from the total and static pressures as $V_p = [2(P_t - P_s)/\rho]^{0.5}$. The total pressure tap was located at the position of the heated probe, with the tip at the location where the center of the heating probe would be. The static tap was a tube with the opening flush with the flow in the tank, in the horizontal plane, and placed in the position of the dummy probe. Because of the flow symmetry, the difference between the two should give an accurate value of the dynamic pressure.

Measurements were made with stirring from the flat-blade impeller, and also with a rotating cylinder. The validity of the pitot tube measurement system was first established by comparison of literature results with the rotating cylinder data. In this work, the tank depth was 18 cm. Results with the flat-blade impeller are presented in Fig. 3, along with the corrected values which incorporate effects of tank depth, mixer to tank depth ratio, and minor pitot tube effects (Tropea et al., 2007). The velocity at the radius corresponding to the centre of the probe can be used for the average shear stress calculations. Fig. 3 shows that the presence of baffles lowers the velocity at relative radius 0.2 to 0.75. Close to the impeller and very close to the wall, the baffle effect is insignificant. Approach velocity to the probe at relative radius r_p/r_{max}= 0.405, for the case with baffles and correction factor k=1.31 for depth, and 1.05 for tube effects, yields V_p/V_{tip}=0.498 or 0.5. This value was used as the average approach velocity in further calculations of the average probe shear stress, and to evaluate the probe Reynolds number.

$$V_p = 0.5\ V_{tip} = 0.5\ (\pi\ D_m\ N/60) \qquad (2)$$

Wall Shear Stress Calculations Wall shear stress over the cylindrical probe is a function of the fluid physical properties, and the local velocity which varies around the probe perimeter. The shear stress profile around the probe can be calculated from the boundary layer theory, which requires knowledge of the approach velocity to the probe, and assumes a flat incoming velocity profile in the axial direction. The average shear stress due to friction (i.e. ignoring form drag) around the probe can be calculated from Equation 3, which was established (Khan et al., 2005) over the Re_p range 1 to 10^5.

$$\tau_w = 2.893\ \rho\ V_p^2\ /\ Re_p^{0.5} \qquad (3)$$

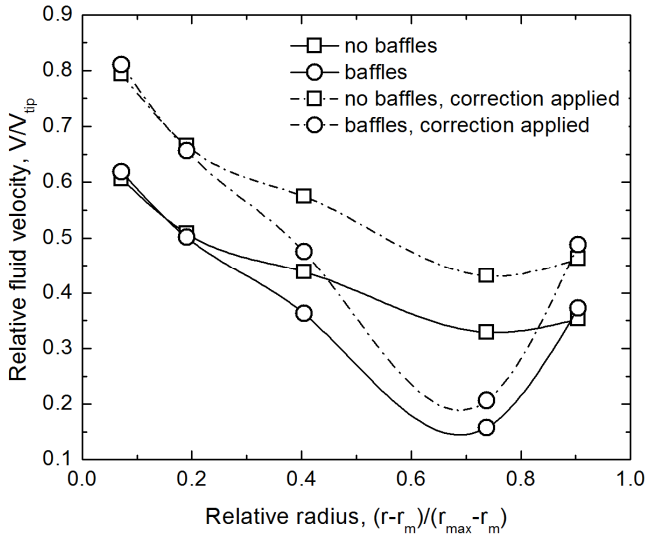

Figure 3 Measured radial velocity profiles using 88.5 mm long impeller, measured in a 177-mm deep tank and corrected to a tank depth of 111 mm.

Clean fluid heat transfer coefficients Heat transfer in the stirred cell unit under clean, non-fouling conditions, was characterized in a series of experiments, using different probes, by varying mixer rotation speed and the bulk and

core temperatures. Film coefficients were determined from the overall heat transfer coefficients using the value of R_w/A_o mentioned above. Results were compared to the Whitaker (1972) equation for heat transfer to a cylinder in free-stream cross flow, where the free-stream approach velocity V_p is used to define the probe Reynolds number :

$$\frac{Nu}{Pr^{0.4}\cdot\left(\frac{\mu_b}{\mu_s}\right)^{0.25}} = \left(0.4Re_p^{0.5} + 0.06Re_p^{0.67}\right) \quad (4)$$

For isolated cylinders in cross flow, at Re ~10, eddies begin to form in the rear of the cylinder, and at Re > 10^3, turbulent eddies are largely responsible for drag. There are two contributions to convective heat transfer from the cylinder; from the undetached boundary layer, and from the wake region (Özışık, 1977). Calculations from the Whitaker equation suggest that as the Reynolds number increases from 2000 to 20,000, the percentage contribution to heat transfer from the undetached boundary layer decreases from roughly 65% to 55% .

In the present case, the approach velocity was calculated from the mixer tip speed using Eqn. 2.. Clean heat transfer data taken using non-fouling Paraflex fluid (Wilson and Watkinson, 1995), are seen in Fig.3 to lie along a line parallel to, but below that of the Whitaker equation. A lower value of V_p/V_{tip} would shift the data closer to that of the Whitaker equation.

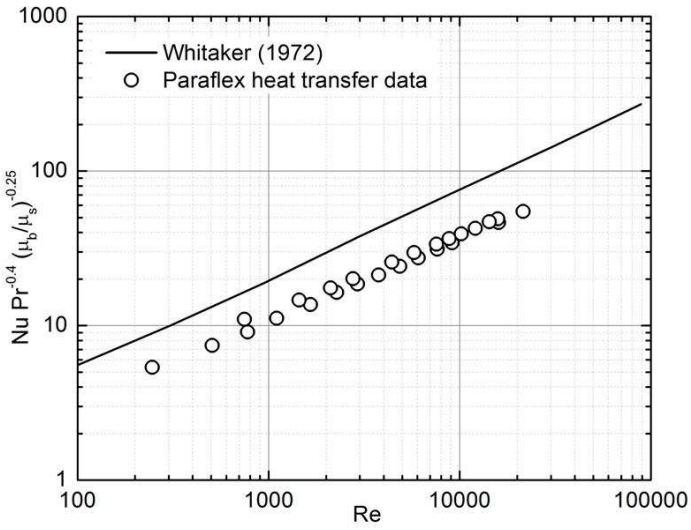

Fig. 4 Clean heat transfer Nusselt group data for fouling probe versus Re_p and compared to Whitaker Eq'n (4)

DEPOSITION EXPERIMENTS IN THE STIRRED TANK UNIT

Fouling with two different ATB feed-stocks Oil samples from two refineries, designated ATB1 and ATB2, with similar suspended solids levels but very different asphaltene contents, were tested, with 1 g/L Fe_2O_3 added. Experiments were run for 24 hours, at T_b = 320°C, probe surface temperatures of 454°C and 505°C, and N = 200 rpm. Results in Table 1 show that at both levels of surface temperatures, ATB1 fouled significantly more (3─6 times) than did ATB2. Since these surface temperatures are in the range for coking, it is not surprising that oil ATB1, with higher percentage of pentane insolubles, and higher Conradson Carbon residue, sulfur, and fixed carbon content than ATB2 should show greater deposition rates. These results show that the stirred tank system can detect fouling differences arising from differences in feed-stocks.

Temperature effects on fouling rate and deposit composition Using a Type 1 probe, the probe temperature was increased in steps, to get a detectable amount of deposit on the surface. Increases of the surface temperature had to be accompanied with increases in the bulk liquid temperature, so that the limited probe heat duty (1000 W) could maintain the temperature difference (T_s–T_b) at high rotation speeds. Deposits were barely measureable at low temperatures, and no deposits were evident on the dummy (q=0) probe. As film temperature was increased above 350°C, deposition rate increased dramatically (Figure 5).

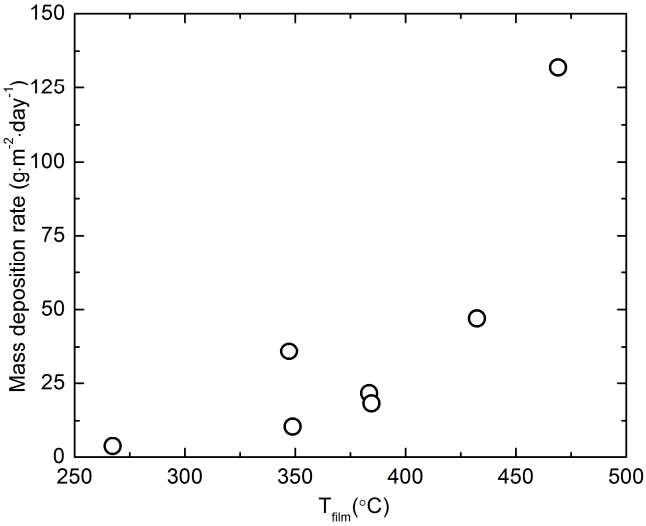

Figure 5 Effect of probe film temperature on deposit mass accumulation rate at 100 rpm, and 1g/l Fe_2O_3 in ATB1

Temperature dependence of the fouling rate involves both bulk and surface temperature effects. Some rate models specifically correlate results separately in terms of both temperatures, and others lump effects into a film temperature. The complicating effect of the liquid viscosity change with temperature has also recently been discussed (Epstein, 2011). In the present case (Figure 6), rates are simply plotted versus the film temperature, and a "fouling activation energy" evaluated from Eq'n (5) was determined as E_f = 53 kJ/mol.

$$\frac{dm}{dt} = a_1 \left(\frac{dR_f}{dt}\right)_{t=0} = a_2 exp\left(-\frac{E_f}{RT_f}\right) \quad (5)$$

This fouling activation energy represents the temperature dependence of the overall fouling process, which may involve several processes including diffusion, mass transfer, and adhesion of iron oxide particles, reaction of coking precursors, etc. Thus, it could vary with shear stress and is not equal to the activation energy of the chemical reaction of coke formation.

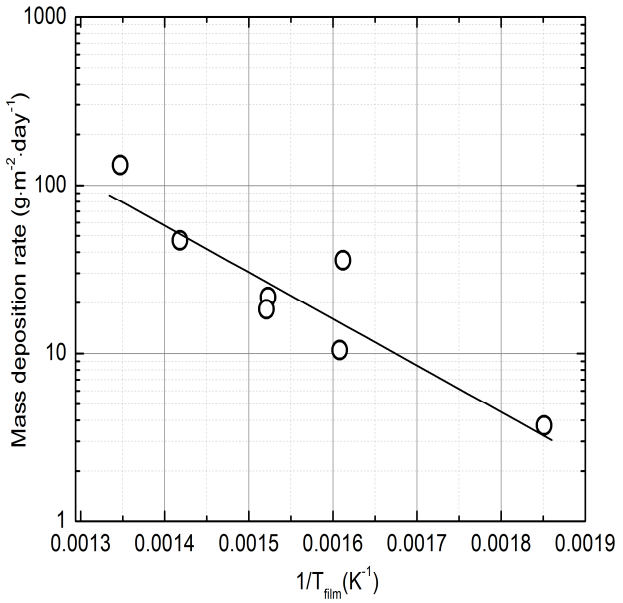

Figure 6 Fouling Arrhenius plot of deposit mass accumulation rate vs. inverse of film temperature

Table 2 shows a consistent effect of film temperature on both deposit amount (after 24 hours) and deposit properties. At the lowest temperature shown, the deposit is very thin and light (10 μm; 42 mg), and high (65%) in ash content. At the highest film temperature values, the deposit is thickest and heaviest (reaching respectively 88 μm and 376 mg), and lowest in ash content (16%). These results suggest that at lower temperatures, both particulate and organic deposition occurs; as temperature is increased, the relative importance of the organic coking reactions is increased, and deposits are enriched in organic content.

Table 2 Deposit Properties at Different Film Temperatures (ATB1, t~24h)

T_{film} (°C)	Deposit Weight (mg)	Deposit Thickness (μm)	Deposit Ash Content (wt.%)	Deposit Organic Content (wt. %)
386	42	10	65	35
417	135	30	46	54
448	376	88	16	84

Table 3 shows EDX analyses of deposit surfaces from a run using ATB2 at low temperature (T_{core}~ 300°C). Samples show averages of about 44 % carbon, 31% iron, 18% sulfur, 6% oxygen and a trace (0.2%) of sodium. These analyses, with roughly 57% inorganic content, are consistent with deposits from a heavy oil doped with iron oxide particles. Although EDX analyses may not represent bulk deposit chemistry, the calculated S/Fe atomic ratios average 1.02, which suggests some sulfidation of the iron oxide to FeS has occurred. Scanning electron microscopy showed the presence of crystal-like materials

Table 3 EDX Analyses of Low Temperature Deposits

Element Conc'n wt. %	Sample A	Sample B
Carbon	42.6	44.7
Oxygen	6.2	6.4
Sodium	0.2	0.3
Sulphur	18.7	18.2
Iron	32.3	30.3
S/Fe (atomic)	1.0	1.04

Effect of Suspended Iron Oxide Concentration Figure 7 shows an unexpected non-linear trend of deposition rate versus iron oxide concentration at two rotational speeds. Whereas transport is expected to vary linearly with particle concentration, particle agglomeration or complex particle attachment (e.g. particle bouncing, dendritic deposition) or removal by abrasion may occur at higher concentrations. Shift of the maximum toward lower concentration, from 3 g/l at 100 rpm to 1 g/l at 200 rpm, may reflect abrasion effects. Further work is needed to explain these results.

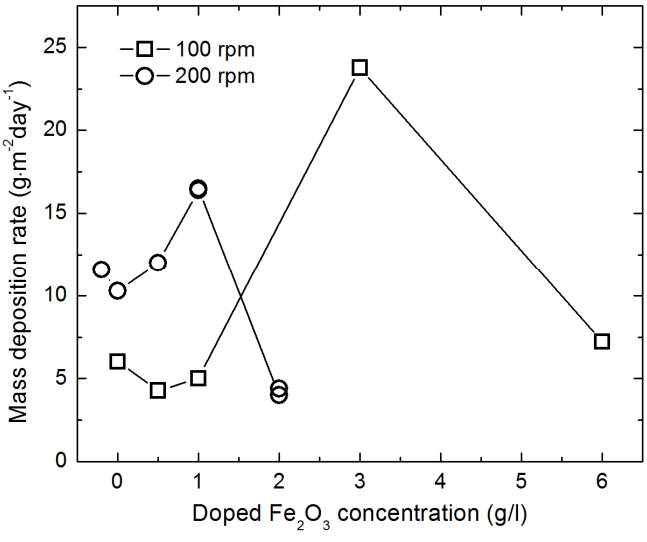

Figure 7 Effect of doped Fe_2O_3 concentration on deposition rates (T_b = 320°C, $T_{s,o}$= 454°C, Re_m (100 rpm) = 3995, Re_m (200 rpm,) = 7990. Value of "– 0.2 g/l" indicates filtered oil without original 0.2 g/l of particles.

Rotation speed and particle size effects on fouling rate Increasing the rotation speed of the stirrer leads to higher

local velocities over the probe, and higher wall shear stress. Results of experiments with both particles sizes (Figure 8) show similar trends of deposition rate with rotational speed: first an increase in rate at low rotational speeds, followed by a decrease in rate at higher rotational speeds. With smaller particles, the maximum occurs at lower rotational speeds.

The trend of increasing deposition rate with velocity up to a maximum, followed by a sharp decrease in fouling rate has been observed in other systems (such as polystyrene fouling, and colloidal particle deposition), and has been interpreted via a particle transfer plus adhesion model (Vašaacute et al., 1995). The initial increase in deposition rate with velocity (rotation speed in the present case) is attributed to the increased mass transfer (particle transport to the probe), and the decreasing trend after the maximum deposition rate may be attributed to lower residence time in the boundary layer (reduced adhesion). In the present case, lower residence time in the wall region could lead to reduced coking. As well, particle removal from the surface could occur at higher shear stress, or particle abrasion may become important. Generally, in fouling under industrial conditions, fouling rate declines with increased flow velocity or wall shear stress (Srinivasan and Watkinson, 2005; Bennett et al., 2009; Joshi et al., 2009) hence the right-hand side of the curve of Figure 8 is most important.

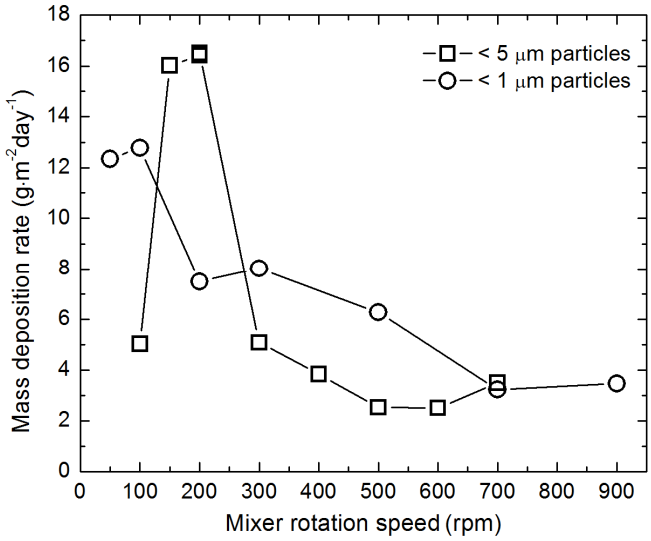

Figure 8 Effect of mixer rotation speed on deposition rates at 1g/L Fe_2O_3, (T_b = 320°C, $T_{s,o}$ = 448 ± 8°C).

The effect of particle size can also be observed in Figure 8. Although results are scattered, on average slightly more deposits were obtained with smaller particles, which could be due to: (i) better particle transport (in diffusion regime, smaller particles give more deposit, (ii) better physico-chemical adhesion for small particles, (iii) less particle removal, (iv) reduced tendency for particle settling in the tank. Particle size effects in asphaltene deposition have been discussed recently (Eskin et al., 2011; Bennett, 2012).

Deposition rate data as a function of rotational speed, can also be re-plotted versus probe Reynolds number or wall shear stress using Equations 2 and 3. Temperature effects on properties of oil were accounted for by empirical equations which fit the reported values in Table 1. The shapes of the plots, given in Figure 9, are similar to those of Figure 8. The slight rise in deposition rate for the highest Re tested is not deemed significant. The range of the Reynolds number is seen to be about 2000 to 16,000, and that of the surface shear stress as 0.7 to 12 Pa. The latter value is in the range for shell and tube heat exchangers in crude oil pre-heat trains (Joshi et al., 2009).

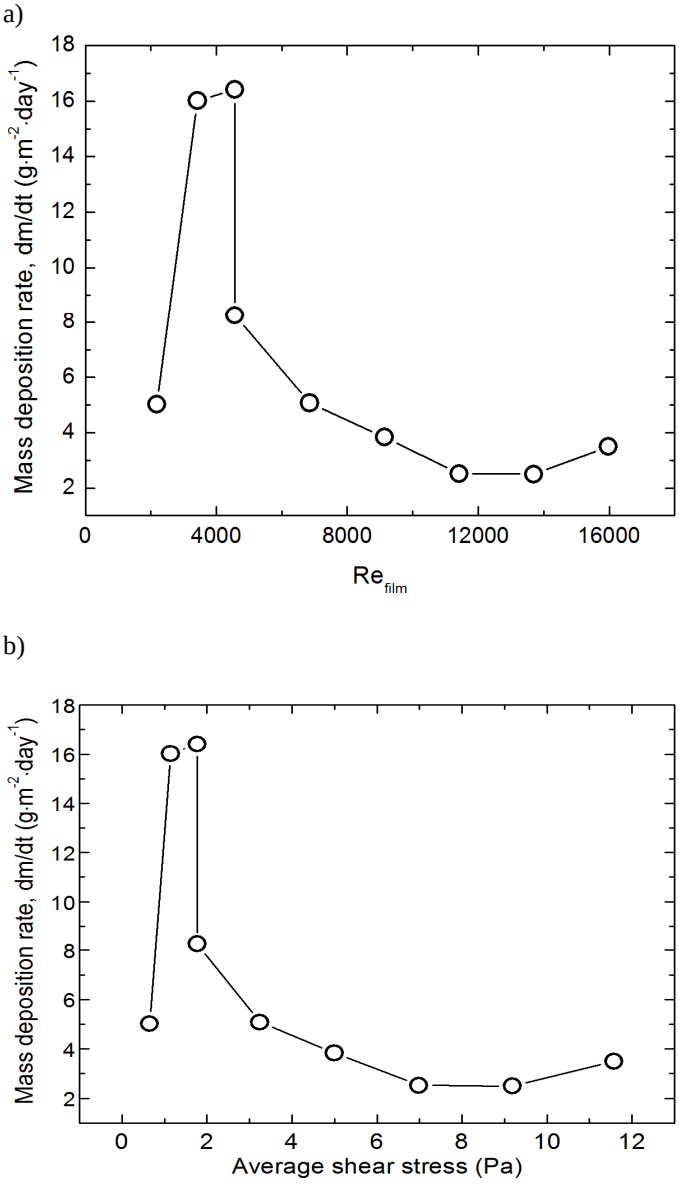

Figure 9 Fouling rates of < 5 micron particles versus a) film Reynolds number based on approach velocity, and b) versus calculated probe wall shear stress.

CONCLUDING REMARKS

1. A stirred-tank fouling test unit which uses about 1.5L of oil/batch has been developed, and evaluated for fouling of atmospheric tower bottoms (ATB) doped with micron sized Fe_2O_3 particles. Fouling is detected on a vertical rod heater with a built-in thermocouple, mounted between the stirrer blade and the tank wall. Under relatively mild conditions, fouling was detected by the thickness or mass of the deposit after about 24 hours. For severe conditions the thermal fouling resistance was also measured.
2. To establish the flow conditions over the heated probe, the velocity field within the unit was established by pitot tube measurements. In the present geometry, the fluid approach velocity to the probe was found to be about 50 percent the tip speed of the stirrer blade. Fouling on the probe was measured over the Reynolds number range 2,000─16,000, which corresponded to wall shear stresses of up to 12 Pa.
3. Over the range of film temperatures (average of probe surface and bulk fluid temperature) of 270─470°C, the fouling activation energy was found to be 53 kJ/mol. At moderate film temperature of 386°C, deposits were comprised of about 35% organic material (arising from the oil), and 65% ash (from the added Fe_2O_3). At a film temperature of 448°C, due to increased coking, deposits were 84% organic and 16% ash. Fouling rates in the stirred tank unit were sensitive to stirrer rotational speed (or probe wall shear stress), and passed through a maximum as the rotational speed was increased as would be expected from transport plus adhesion models. Concentration effects were complex, showing an expected increase only over a limited range. Oil ATB1, gave higher fouling rates than ATB2, reflecting the higher pentane insolubles content (5.8% vs. 1.4%) of the former.
4. The test unit shows promise for determining effects on deposition rate of wall and bulk temperatures, shear stress, pentane insolubles and possibly other impurities in an oil. Deposits are accessible for examination. With minor improvements, higher pressures, temperatures and wall shear stress values can be reached.

ACKNOWLEDGEMENTS

This work was supported by Phillips 66. The authors appreciate the contributions of Keith Lawson, Bruce Newman and David Henning to the development of the system, and to the experimental program. Yonghua Li built the original apparatus and carried out the early experimentation at the University of British Columbia.

NOMENCLATURE

a_1, a_2 constants defined in Eq'n 5
A_o external heated probe surface area (m^2)
ATB1 atmospheric tower bottom sample 1
ATB2 atmospheric tower bottom sample 2
b velocity exponent for film heat transfer coefficient
C_p heat capacity of liquid (kJ/kg K)
d_p particle diameter (m)
D_m mixer diameter (m)
D_p probe diameter (m)
E_f fouling activation energy defined using film temperature (kJ/mol)
f friction factor (-)
g acceleration due to gravity (m/s^2)
h film heat transfer coefficient (kW/m^2K)
ID tank inside diameter (m)
k correction factor for pitot tube (-)
m deposit mass per unit area (kg/m^2)
N rotational speed (revolutions/minute)
Nu Nusselt number, hD_p/λ (-)
P pressure (Pa)
Pr Prandtl number, $C_p\mu/\lambda$ (-)
q heat flux (kW/m^2)
r radial position (m)
r_m mixer radius (m)
r_{max} radius of tank (m)
r_p radial position for centerline of probe (m)
R_f thermal fouling resistance (m^2K/kW)
R_w thermal resistance of probe wall (m^2K/kW)
Re_m mixer Reynolds number, $V_{tip} D_m/\nu$ (-)
Re_p probe Reynolds number, V_pD_p/ν (-)
t time (s)
T_b bulk fluid temperature (K)
T_{core} measured core temperature (K)
T_{film} film temperature (K), average of T_b and $T_{s,o}$
T_s calculated probe surface temperature (K)
$T_{s,o}$ initial probe surface temperature (K)
U overall heat transfer coefficient (kW/m^2K)
V_p approach velocity to probe (m/s)
V_{tip} tip velocity of mixer (m/s)
x deposit thickness (m)

λ thermal conductivity of fluid (kW/mK)
μ viscosity (Pa·s)
ν kinematic viscosity (m^2/s)
ρ density (kg/m^3)
τ_w shear stress at probe wall (Pa)

Subscripts
b bulk
s surface
d deposit
core measured at heater core
film evaluated at film temperature
max maximum value

REFERENCES

Akbarzadeh, K., Eskin, D., Ratulowski, J. and Taylor, S., 2012, Asphaltene Deposition Measurement and Modeling for Flow Assurance of Tubings and Flow Lines, *Energy & Fuels*, Vol. 26, pp. 495-510.

Bennett, C. A., 2012, A Theory Describing Asphaltene Adhesion Fouling Inside Heat Exchanger Tubes, *Heat Transfer Engineering*, Vol. 33, pp. 1246-1250.

Bennett, C. A., Kistler, R. S., Nangia, K., Al-Ghawas, W., Al-Hajji, N. and Al-Jemaz, A., 2009, Observation of an Isokinetic Temperature and Compensation Effect for High-Temperature Crude Oil Fouling, *Heat Transfer Engineering*, Vol. 30, pp. 794-804.

Epstein, N., 2011, Comments on "Relate Crude Oil Fouling Research to Field Fouling Observations by Joshi et al.", *Proc. International Conference on Heat Exchanger Fouling and Cleaning - 2011*, Crete Island, Greece, pp. 62-64.

Eskin, D., Ratulowski, J., Akbarzadeh, K. and Pan, S., 2011, Modelling asphaltene deposition in turbulent pipeline flows, *The Canadian Journal of Chemical Engineering*, Vol. 89, pp. 421-441.

Fan, Z., Rahimi, P., McGee, R., Wen, Q. and Alem, T., 2010, Investigation of Fouling Mechanisms of a Light Crude Oil Using an Alcor Hot Liquid Process Simulator, *Energy & Fuels*, Vol. 24, pp. 6110-6118.

Fernández-Seara, J., Uhía, F. J., Sieres, J. and Campo, A., 2007, A general review of the Wilson plot method and its modifications to determine convection coefficients in heat exchange devices, *Applied Thermal Engineering*, Vol. 27, pp. 2745-2757.

Joshi, H. M., Shilpi, N. B. and Agarwal, A., 2009, Relate Crude Oil Fouling Research to Field Fouling Observations, *Proc. International Conference on Heat Exchanger Fouling and Cleaning VIII - 2009*, Schladming, Austria, pp. 15-16.

Khan, W. A., Culham, J. R. and Yovanovich, M. M., 2005, Fluid Flow Around and Heat Transfer From an Infinite Circular Cylinder, *Journal of Heat Transfer*, Vol. 127, pp. 785-790.

Özışık, N., 1977, *Basic heat transfer*, McGraw-Hill Companies, New York, NY U.S.A..

Srinivasan, M. and Watkinson, A. P., 2005, Fouling of Some Canadian Crude Oils, *Heat Transfer Engineering*, Vol. 26, pp. 7-14.

Stephenson, T., Kubis, A., Derakhshesh, M., Hazelton, M., Holt, C., Eaton, P., Newman, B., Hoff, A., Gray, M. and Mitlin, D., 2011, Corrosion-Fouling of 316 Stainless Steel and Pure Iron by Hot Oil, *Energy & Fuels*, Vol. 25, pp. 4540-4551.

Tropea, C., Yarin, A. L. and Foss, J. F., 2007, *Springer Handbook of Experimental Fluid Mechanics*, Springer.

Vašaacute, k, F., Kaštánek, F., Bowen, B. D., Chen, C. Y. and Epstein, N., 1995, Fine particle deposition in laminar and turbulent flows, *The Canadian Journal of Chemical Engineering*, Vol. 73, pp. 785-792.

Whitaker, S., 1972, Forced convection heat transfer correlations for flow in pipes, past flat plates, single cylinders, single spheres, and for flow in packed beds and tube bundles, *AIChE Journal*, Vol. 18, pp. 361-371.

Wilson, D. I. and Watkinson, A. P., 1995, Model experiments of autoxidation reaction fouling. I: Mechanisms, *Chem. Eng. Res. Des*, Vol. 73, pp. 59-68.

Young, A., Venditti, S., Berrueco, C., Yang, M., Waters, A., Davies, H., Hill, S., Millan, M. and Crittenden, B., 2009, Characterization of Crude Oils and Their Fouling Deposits Using a Batch Stirred Cell System, *Proc. International Conference on Heat Exchanger Fouling and Cleaning VIII - 2009*, Schladming, Austria, pp. 17-26.